4-1-2004

Lubricant Pyrolysis During Sintering of Powder Metallurgy Compacts

M. M. Baum

R. M. Becker

A. M. Lappas

J. A. Moss

Diran Apelian
Worcester Polytechnic Institute, dapelian@wpi.edu

See next page for additional authors

Lubricant Pyrolysis during Sintering of Powder Metallurgy Compacts

M.M. BAUM, R.M. BECKER, A.M. LAPPAS, J.A. MOSS, D. APELIAN, D. SAHA, and V.A. KAPINUS

The chemistry surrounding the pyrolysis of *N,N′*-ethylenebisstearimide (EBS) compacted with iron powder is described for the first time. Heat treatment is carried out in a 5 vol pct hydrogen atmosphere (balance nitrogen) over the 100 °C to 850 °C range. The exhaust from the furnace is monitored by Fourier transform infrared and dispersive ultraviolet absorption spectroscopy; condensable materials are analyzed by gas chromatography/mass spectrometry (GC/MS). A wide range of analytes emitted from the preceding process were characterized. The aliphatic CH stretch in the 3000 to 2700 cm^{-1} range and the asymmetric CO stretch in gaseous CO_2 at 2350 cm^{-1} are excellent indicators of the extent of delubrication. A bimodal CO emission phase is observed in the temperature window between delubrication and sintering. Three major large molecule reaction products, along with five minor compounds, are identified by GC/MS. A preliminary reaction mechanism is inferred based on product analysis and known organic chemistry. It appears that hydrolysis of EBS competes with γ-H abstraction yielding an *N*-vinyl amide and stearamide, which undergoes further reaction. Hydrolysis affords stearic acid, which decarboxylates to heptadecane, and 2-heptadecyl-4,5-dihydroimidazole *via* ring closure of the corresponding amino-amide.

I. INTRODUCTION

LUBRICANTS have become essential in powder metallurgy (PM) parts production. They are typically admixed (0.5 to 1.5 wt pct) with the metal powder to aid compaction uniformity and to decrease die-wall friction during compaction and ejection, thereby reducing die wear. Lubricants can also act as temporary binders to enhance the "green" strength of a metal part.[1] The lubricant remaining on and within the compact may restrict densification during processing and must be removed in the early stages of heating. Delubrication commonly is achieved in the first zone of a sintering furnace by heating the part to temperatures in the 500 °C to 600 °C temperature range at a fixed rate and under controlled atmospheric conditions; this strategy minimizes defects, carbon contamination, and compact deformation.[2] The delubricated part then enters the second zone (commonly in the 1200 °C to 1300 °C temperature range) for sintering. The third zone cools the sintered part at a desired rate to obtain the requisite microstructural properties. Controlled delubrication is imperative toward achieving high-quality parts for the following reasons: the elevated thermal gradient at the transition between the first and second zones can cause parts to expand rapidly and develop microscopic fissures ("blistering"); improper gas flows and belt speeds can lead to carbon deposition on the part and at the grain boundaries ("sooting"); delubrication products deposit throughout the furnace, even in the coolers, which are far removed from the preheating chamber,[3] leading to significant maintenance costs; and pollutants emitted in the exhaust stream of furnaces operating inefficiently are increasingly of environmental concern.

In practice, lubricant removal is difficult to control, which often leads to reduced yields in PM manufacturing processes. Throughput is another important issue: process control ideally should lead to a delubrication cycle that yields defect-free parts in a minimum of furnace time, thereby increasing productivity and reducing the net energy consumption. Efficient process control requires rapid monitoring of suitable indicators, preferably gas-phase products of delubrication. *N,N′*-Ethylenebisstearimide (EBS), shown in Figure 1, is the lubricant of choice in many modern iron PM processes because it possesses all the necessary properties for compaction and thermolyzes relatively cleanly in a range of furnace atmospheres. The process parameters influencing the removal of EBS from compacted iron parts have been discussed in the literature.[4,5] A number of complex chemical and physical processes can be expected to occur, often simultaneously, between the onset of lubricant thermolysis and sintering. These include the decomposition of organic species; chemical interactions between these species and the surfaces of the compacted metal powders; mass transport of reactants, volatile species, and degradation products through lubricant-filled and empty pores; and changes in the distribution of liquid-phase lubricant within the pore structure of the compact. Although thermal delubrication of PM compacts has been practiced for many years, a basic understanding of the associated chemical processes is still lacking.

For the first time, the chemical mechanism describing the pyrolysis of EBS in iron PM compacts is described. Preliminary data from our study suggest that EBS decomposes *via* a series of competing reactions, including EBS hydrolysis to stearic acid, followed by decarboxylation.[6] The purpose of this article is to provide a full account of these, and more

This paper is dedicated to Robert M. Becker. Bob died tragically in an automobile accident in December 2003. He was a good friend and valued colleague who will be greatly missed.

M.M. BAUM, Associate Faculty Member, R.M. BECKER, Research Scientist, A.M. LAPPAS, Visiting Associate, and J.A. MOSS, Assistant Faculty Member, are with the Department of Chemistry, Oak Crest Institute of Science, Pasadena, CA 91107. Contact e-mail: m.baum@oak-crest.org D. APELIAN, Professor, and D. SAHA, Ph.D. Student, are with the Metals Processing Institute, Worcester Polytechnic Institute, Worcester, MA 01609. V.A. KAPINUS, Ph.D. Student, is with the Division of Chemistry and Chemical Engineering, California Institute of Technology, Pasadena, CA 91125.

Manuscript submitted September 9, 2003.

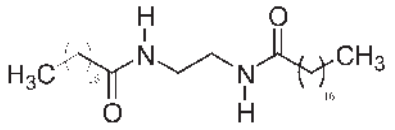

Fig. 1—Chemical structure of EBS.

recent, results. Quantitative product analysis using a combination of Fourier transform infrared (FTIR) absorption spectroscopy and gas chromatography/mass spectrometry (GC/MS) is used to discuss potential reaction pathways, as well as the implications of these measurements on the development of process control sensors and the design of the next generation of PM lubricants.

II. EXPERIMENTAL PROCEDURE

The research described here was carried out between 2000 and 2003 in two principal experimental phases, as discussed in Sections A and B. Authentic samples of EBS were obtained commercially (Sigma-Aldrich, St. Louis, MO) and used without further purification. The characteristics of the iron PM compacts, shown in Table I, were invariant in three sample batches prepared over the course the study, and are identical to those used previously.[5]

A. *Experimental Design, Phase I*

The experimental setup used in phase I (2000 Study) to monitor the gas-phase products emitted from iron-EBS compacts upon heat treatment is shown schematically in Figure 2. The output from a cylinder containing 5 vol pct hydrogen (H_2) in 95 vol pct nitrogen (N_2) is flowed at 2 L min^{-1} through 6.4 mm (0.25-in.) outside diameter (OD) perfluoroalkoxy (PFA) tubing and delivered to a custom, all-quartz furnace containing the iron compact. The furnace is 400-mm long with a diameter of 73 mm. The inlet to the furnace consists of a 65/40 spherical-ground joint, tapered down to 12-mm OD tubing at the inlet, to allow convenient access to the furnace interior. The distal end of the furnace narrows to a zone containing a quartz wool filter and tapers down further to 12-mm-OD tubing. The furnace is connected to the tubing by means of suitable PFA compression fittings. A thermal well at the center of the furnace accommodates a K-type thermocouple, which is located within 10 mm of the compact. The furnace is heated by a high-temperature beaded heater and insulated by ceramic sheeting. Digital temperature controllers are used throughout to manage the thermal environment of the various apparatus sections.

The gas flow exiting from the furnace is evenly split (*i.e.,* two flows of 1 L min^{-1} each), and directed to a pair of spectrometers.

1. A Fourier transform infrared spectrometer (Magna-IR 560, Nicolet, Madison, WI) equipped with a liquid nitrogen-cooled mercury-cadmium-telluride detector: a 5-m optical pathlength (OPL) multipass cell of the White design[7] (Model 16-V, Infrared Analysis, Inc., Anaheim, CA) located in the sample chamber of the spectrometer is maintained at 120 °C to avoid condensation on the gold-coated mirrors and the zinc selenide windows. Spectra in the 6000 to 650 cm^{-1} range are recorded at a resolution of 4 cm^{-1} with 32-sample averaging.
2. A dispersive ultraviolet-visible (DUV-vis) 2048 element CCD array spectrometer (S2000, Ocean Optics, Dunedin, FL): a 0.5-m OPL single-pass cell equipped with a pair of quartz windows at either end is maintained at 120 °C to avoid condensation on the optics; the double window approach prevents heat loss from the window in contact with the sample. The radiation from a deuterium source (L6565, Hamamatsu Corp., Bridgewater, NJ) is collimated through the cell and focused onto the entrance slit of the spectrometer. Spectra in the 185 to 510 nm window are recorded at a full-width half-maximum (FWHM) spectral resolution of 0.84 nm at 253.65 nm with an array integration time of 10 ms and 15,000 sample averaging.

Table I. Characteristics of Carbonyl Iron Powder

Iron Powder	Characteristics
Designation	carbonyl iron powder
Supplier	Hoeganaes Corporation
Average iron particle size (μm)	80
Shape	rectangular bar
Dimensions, $w \times d \times l$ (mm)	$13 \times 13 \times 32$
Typical mass (g)	37
Density (g cm^{-3})	7.05
C content (ppm w)	8000 (Asbury 3203 graphite)
N content (ppm w)	10
O content (ppm w)	1500
S content (ppm w)	100
Lubricant	EBS
Average lubricant particle size (μm)	15
Lubricant content (wt pct)	1

The PFA transfer line connecting the furnace exhaust to the spectrometer sample cells is maintained at approximately 60 °C by a self-limiting heater. The exhaust from the cells is directed to a fume hood.

In experiments conducted in a hydrated atmosphere, the three-way valve is turned to sparge the carrier gas through distilled water (H_2O) in a temperature-controlled (55 °C) Pyrex-bubbler, fitted with a fritted dispersion tube, in a manner analogous to Renowden and Pourtalet.[8] The gas line between the bubbler and the furnace is heated to avoid water condensation. Thus, experiments are either carried out under anhydrous conditions or in an atmosphere containing approximately 12 vol pct H_2O.

In a typical experiment, the metal compact is evenly heated at a rate of 10 °C min^{-1}, from 100 °C to 600 °C, under a flowing N_2/H_2 (95-5 by volume) atmosphere. The instruments are synchronized at 2.5-min duty cycles, resulting in the acquisition of 20 spectra per spectrometer per experiment. Data are stored in independent PCs and postprocessed (*vide infra*). The release of a white particulate material is routinely observed above 400 °C and gradually condenses on the optics, which require cleaning after every second experiment. Transfer lines routinely are blown out with N_2 to remove any residues. In one run, the white material was condensed on an optical-grade potassium bromide plate for analysis by FTIR spectroscopy (256 scans, 4 cm^{-1} resolution).

Six runs were carried out, three under anhydrous conditions and three under hydrated conditions, as well as numerous controls, including thermal decomposition studies on EBS (50 mg, 8.4×10^{-5} mol) in the absence of iron powder.

B. *Experimental Design, Phase II*

The experimental setup used in phase II (2002 Study) to monitor the gas-phase products of iron-EBS compacts upon heat treatment is shown schematically in Figure 3 using a N_2/H_2 (95-5 by volume) atmosphere flowing at 1 L min^{-1}. The principal differences with respect to the phase I experiments are discussed subsequently. The UV-vis measurements are omitted. The multipass cell is replaced by the single-pass cell used previously for UV-vis measurements to allow higher temperatures (200 °C) to be used, to reduce condensation on the optics; TEFLON* and TEFLON-coated Viton O-rings are used to seal the system at these elevated temperatures. The transfer line between the furnace and the sample cell was shortened (<35 cm) and controlled to 200 °C to minimize deposition in the IR sample cell. Condensable materials are collected directly at the exhaust of the sample

*TEFLON is a trademark of E.I. DuPont de Nemours.

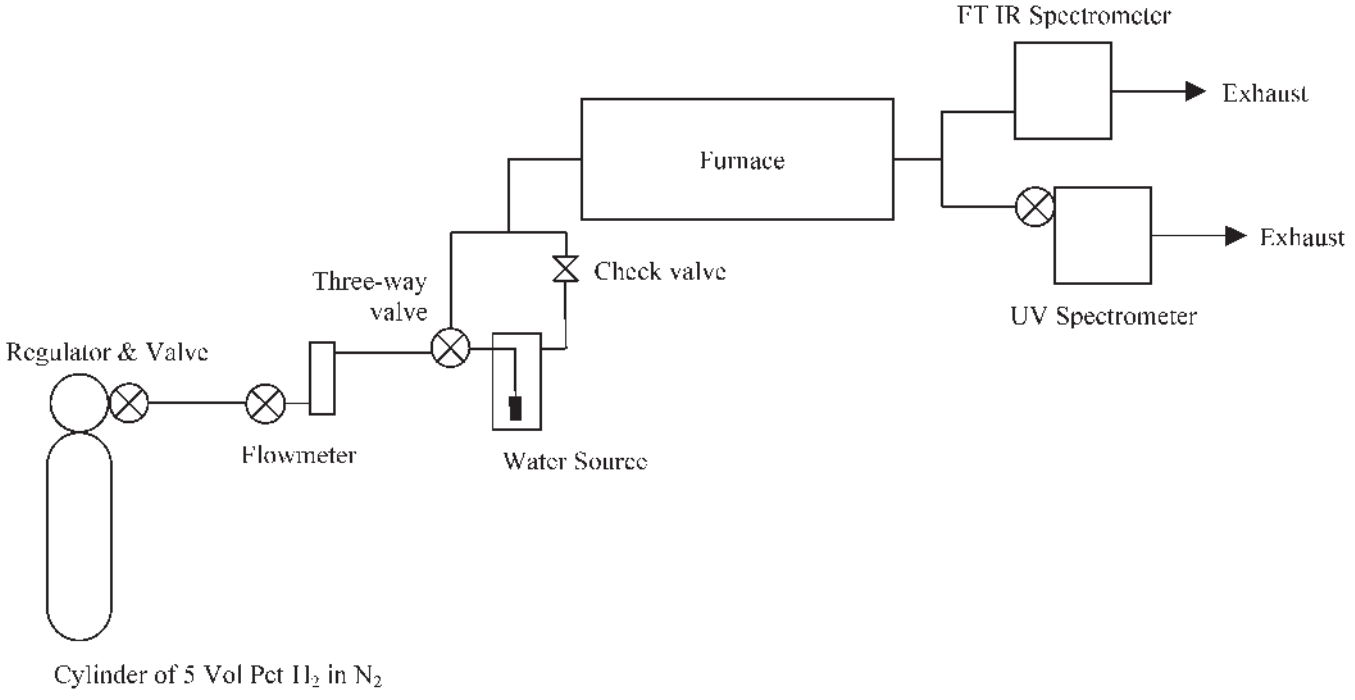

Fig. 2—Schematic representation of the apparatus used in phase I.

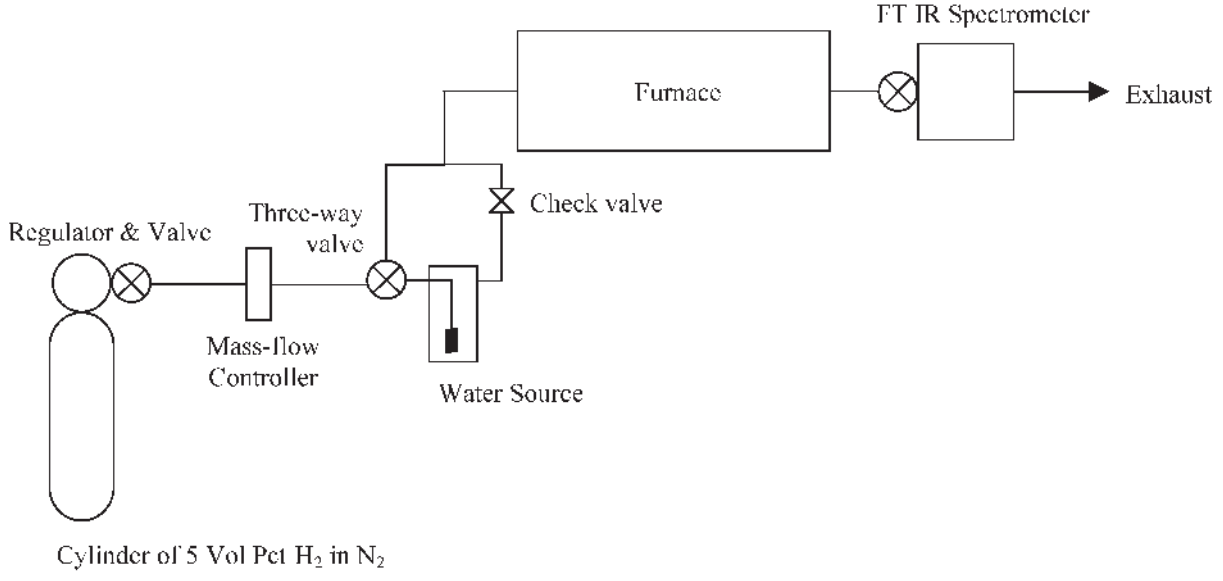

Fig. 3—Schematic representation of the apparatus used in phase II.

Table II. Summary of GC/MS Data Collected on the White Solids (Phase II Experiment, Anhydrous Conditions) Condensed onto Potassium Bromide Window (Figure 8)

Retention Time (min)	T = 410 °C to 430 °C Fractional Area (Pct)	T = 450 °C to 467 °C Fractional Area (Pct)	Observed m/z	Best Library Match	Quality of Match (Pct)
23.64	50.5	41.3	309	2-heptadecyl-4,5-dihydroimidazole	78
21.95	30.4	15.7	280	2-heptadecyl-4,5-dihydroimidazole	78
20.13	7.5	12.2	265	octadecanenitrile	98
18.18	4.1	5.0	255	heptadecanenitrile	81
16.05	2.8	4.7	241	heptadecane	90
14.93	0.8	3.2	227	hexadecane	91
14.85	0.6	2.7	225	1-hexadecene,	90
				1-hexadecanol, or	90
				5-octadecene	90
13.74	0.7	2.1	212	pentadecane	87
				heptadecane	83

cell on optical-grade potassium bromide plates for post-analysis by FTIR spectroscopy (*vide supra*). The material is then dissolved in analytical grade dichloromethane (2 × 1 mL) and injected (15 μL) onto an HP-1 column (30 m) of a model 5890 gas chromatograph (Hewlett-Packard, Palo Alto, CA). The gas chromatograph is coupled to a model 5972 mass sensitive detector (Hewlett-Packard). Mass spectra of the principal components were compared to library spectra in the Wiley138 database, which contains over 137,000 entries. The quality of the library match is included for the eight most abundant products (Table II). In a typical experiment, three samples are collected in the following temperature windows: 250 °C to 380 °C, 405 °C to 430 °C, and 550 °C. The compact mass loss during an experiment was recorded using an analytical balance.

C. *Signal Processing*

Stored IR and UV spectra are analyzed with a least-squares fitting algorithm based on the singular value decomposition theorem, which has been shown previously to be highly effective in extracting spectral features from a complex mixture over a range of applications.[9,10,11] The measurement apparatus is calibrated and evaluated by connecting the sample cell to a gas manifold system. Synthetic mixtures (carbon dioxide, CO_2, carbon monoxide, CO, and ammonia, NH_3) of known concentration are prepared by blending certified gases using mass flow controllers. The exhaust from the blending system is flowed through the sample cell at 1 L min^{-1}. The concentrations of the calibration mixtures are chosen to span the measurement range at equal intervals; four to five concentrations are used in a typical run. A plot of the known concentration of the calibration sample (actual concentration) *vs* the concentration calculated by the analyzer based on the pattern recognition fit (observed concentration) affords a polynomial calibration curve (Figure 4); first- and second-order curves generally provide good fits. The calibration curves correct instrument readings for deviations from ideal Beer–Lambert behavior, which are common when the measured absorption feature is much narrower than the spectral resolution of the detector.[12,13]

In the case of methane (CH_4) and ethene (C_2H_4), high-resolution library spectra recorded at 120 °C (the temperature of the sample cell in phase I) are employed to estimate

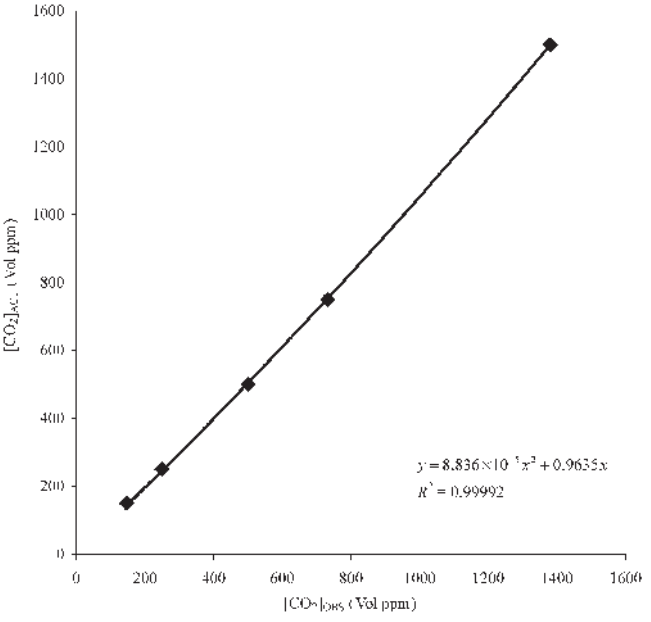

Fig. 4—Calibration curve for CO_2 in phase II.

concentrations. The reference spectra are deresolved to match the resolution used in our experiments and the area of the appropriate peak is compared to its counterpart in the mixtures. Note that the absolute accuracy of this approach is expected to be lower than when calibration standards are employed, but the relative accuracy should be unaffected.

III. RESULTS

A. *Product Analysis*

The FTIR and DUV-vis absorption spectroscopy on gas-phase emissions formed upon heat treatment of iron-EBS parts in the 200 °C to 600 °C range identified the presence of two major species (Figure 5): carbon dioxide (CO_2), ν_{max} 2359 and 2339 cm^{-1} (C=O), and product(s) with a strong hydrocarbon absorption band, ν_{max} 2968 (CH_3), 2933 (CH_2), and 2864 cm^{-1} (CH_2). Carbon monoxide, ν_{max} 2176 cm^{-1}

(C=O), CH_4, ν_{max} 3016 cm^{-1} (CH), C_2H_4, ν_{max} 949 cm^{-1} (CH) (Figures 5 and 6), and ammonia (NH_3), λ_{max} 200.9, 204.7, and 208.5 nm (n-σ*), were measured as minor products at levels approximately one order of magnitude lower than corresponding CO_2 concentrations.

The long wavelength IR spectral window (Figure 6) of this gas-phase sample also revealed a number of significant bands that could be assigned to an amide C=O bond, as well as a pair of peaks characteristic of the vinyl group (*vide infra*).

The IR spectra, along with band assignments (Table III), of the white solid collected during both experimental phases are shown in Figures 7 and 8. A discussion of these data is given subsequently. Gas chromatograph/mass spectrometry analysis of the condensable material collected over two temperature ranges in phase II yielded the data shown in Table II for peaks with a fractional area exceeding 1 pct in either of the samples. The fractional area is calculated from the integrated MS signal for all ions in each peak in the chromatogram and gives a qualitative relative concentration in the sample. Three principal products are obtained, along with five minor products. Characterization of these peaks is provided in Section IV as part of the mechanistic discussion.

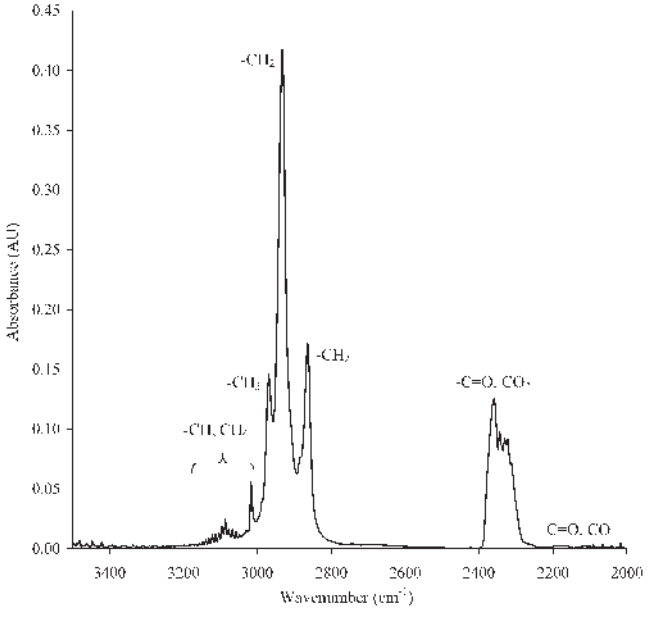

Fig. 5—Absorption bands (phase I experiment, anhydrous conditions, T = 540 °C) due to major pyrolysis products.

Table III. IR Bands of Condensable Products of Pyrolysis Corresponding to Figure 7

Peak	Peak Location, ν_{max} (cm^{-1})	Peak Assignment[38]
A	3200	4,5-dihydroimidazole NH[43]
B	3033	alkene CH, asym.* vib.**
C	2921	alkane CH_2, asym. vib.
D	2851	alkane CH_2, sym.*** vib.
E	2655	unknown
F	1600	alkene C=C, 4,5-dihydroimidazole C=N[42]
G	1468	alkane CH_3, asym. bend alkane CH_2, sci.
H	1443	alkane CH_3, asym. bend alkane CH_2, sci.**** amide CNH, stretch-bend
I	1402	amide CN
J	1287	amide CNH, stretch-open
K	1252	amide CNH, stretch-open

*asymmetric
**vibration
***symmetric
****scissor

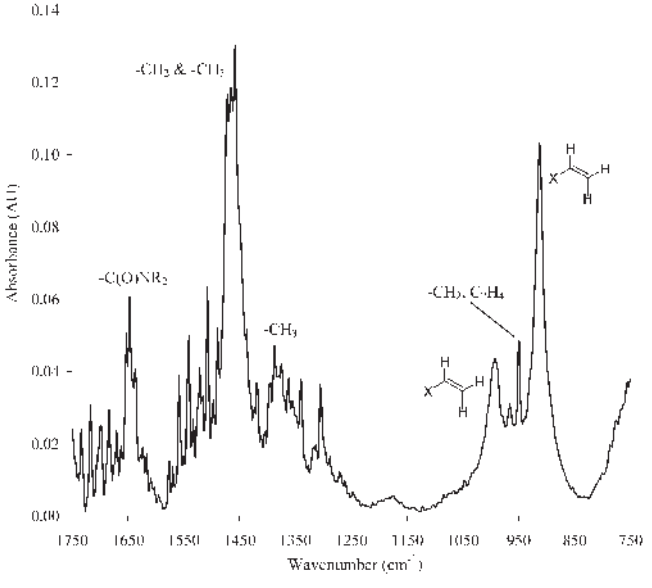

Fig. 6—Absorption bands (phase I experiment, anhydrous conditions, T = 485 °C) due to minor pyrolysis products.

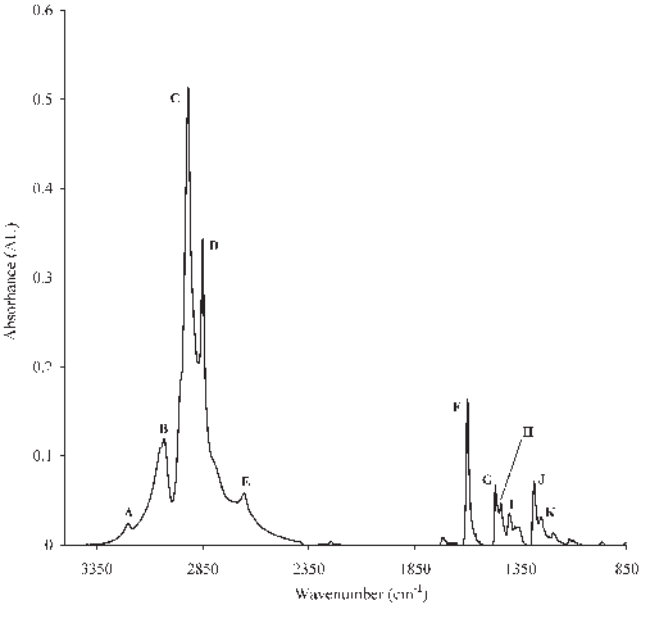

Fig. 7—White solid (phase I experiment, anhydrous conditions) condensed onto potassium bromide window.

B. *Product Emission Profiles*

Product emissions from a thermolyzed iron-EBS compact as a function of temperature are shown in Figures 9 and 10. These emission profiles were highly repeatable, and were statistically invariant as a function of sample preparation date or processing atmosphere water content. A characteristic temperature (T_c), corresponding to half of the total lubricant weight loss, of 450 °C was estimated based on the emissions maximum during heat treatment (Figure 9). Delubrication consistently occurred at approximately 450 °C for all experiments. The magnitude of CO_2 and CO emissions at T_c generally varied by less than ±20 pct as a function of processing atmosphere humidity content or sample preparation date.

In phase II, the processing temperature was increased to 850 °C, which led to the bimodal CO emission phase shown in Figure 11.

IV. DISCUSSION

A. *Lubricant Pyrolysis Emission Profile*

Absorption spectroscopy as well as GC/MS has only seen limited use in studying lubricant thermolysis in mate-

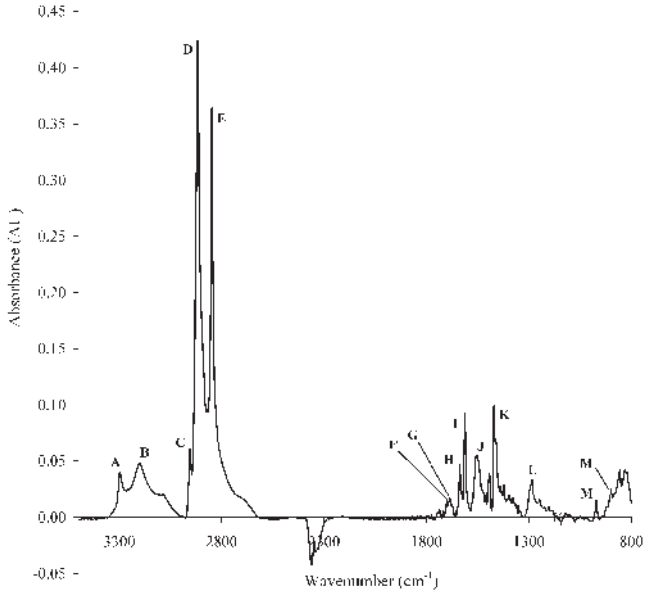

Fig. 8—White solids (phase II experiment, anhydrous conditions, 407 °C < T < 429 °C) condensed onto potassium bromide window.

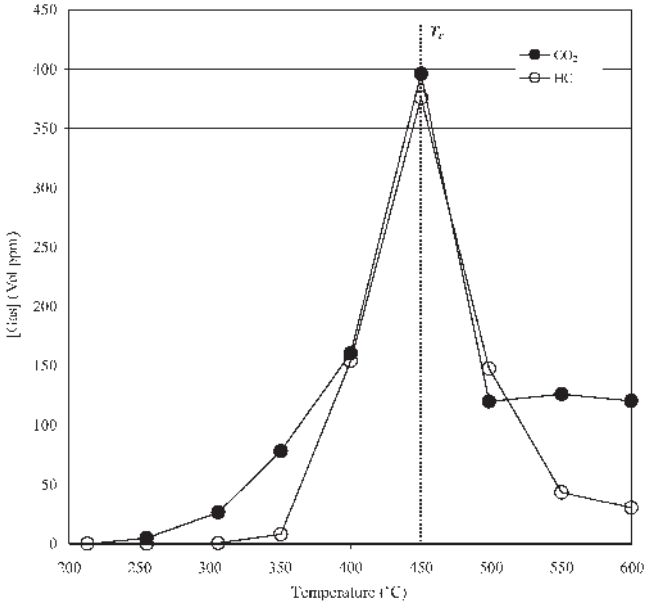

Fig. 9—Product emission profile (phase II experiment, anhydrous conditions) of major pyrolysis products.

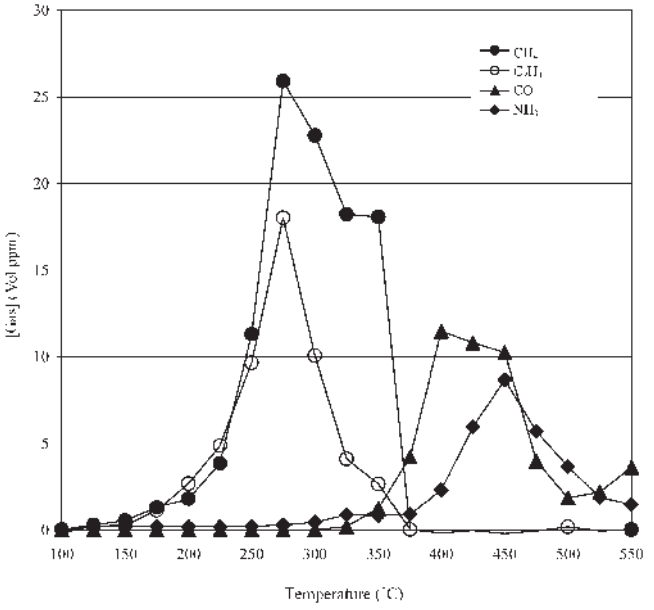

Fig. 10—Product emission profile (phase I experiment, anhydrous conditions) of minor pyrolysis products.

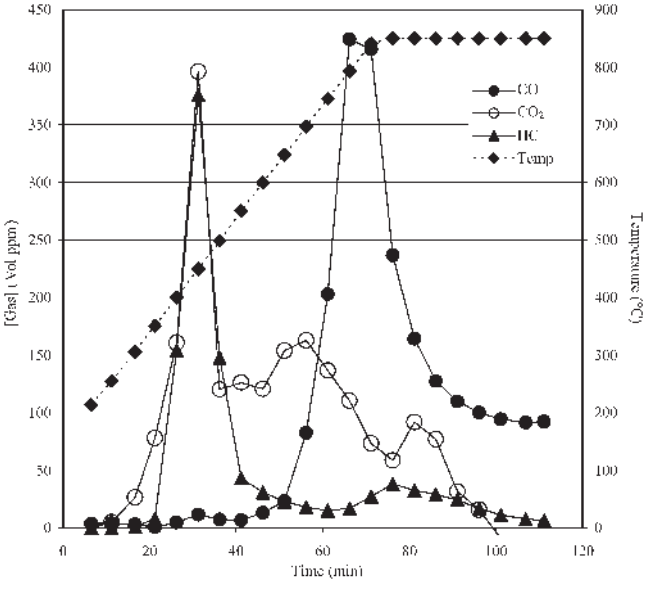

Fig. 11—Product emission profile (phase II experiment, anhydrous conditions) of pyrolysis products between 200 °C and 850 °C. Note that the concentration of the product(s) with a strong C-H stretch (HC) is in arbitrary units.

rial science. Lombardo and co-workers employed TGA in combination with FTIR absorption spectroscopy to study poly(vinylbutyral) burnout kinetics from barium titanate multilayer ceramic capacitors with platinum metal electrodes.[14,15] Binder decomposition was studied as a function of gas-phase emissions including carbon dioxide (2350 cm^{-1}) as well as species containing carbonyl C=O (1680 to 1750 cm^{-1}), CH (2700 to 3000 cm^{-1}), and hydroxyl OH (3550 to 3650 cm^{-1}) functional groups. However, detailed product analysis was not carried out and the concentration of the identified compounds was not estimated in the exhaust stream.

In an isolated account, the gas-phase products of EBS thermolysis have been monitored by FTIR absorption spectroscopy.[16] White and Nayar observed a range of functional groups (*e.g.,* NH, CH_3, and CH_2) at different furnace temperatures, but only identified the small-molecule components (CO_2, CO, and CH_4), leaving the bulk of the reaction products uncharacterized. In addition, the study was limited to pure EBS, which is likely to thermolyze differently than when the lubricant is incorporated into a PM compact.

For the first time, our FTIR measurements on the pyrolysis products of iron-EBS compacts conclusively identified CO_2, CO, CH_4, and C_2H_4 (Figures 5 and 6) and used the measurements to accurately monitor the concentration of these gases of as a function of furnace temperature (Figures 9 through 11). Our results indicate that CO_2 is the principal reaction product out of this set (Figure 9), with CO, CH_4, and C_2H_4 being produced in significantly lower amounts (Figure 10). Large-molecule products are also emitted in significant amounts in tandem with CO_2, peaking at 450 °C.

Thermogravimetric analysis measurements in our laboratories,[5] and by others,[4,17] on lubricant burnout from iron-EBS PM compacts have estimated a T_c around 450 °C, with completion of this delubrication event under 475 °C. The temperature corresponding to the emission maximum of the principal delubrication products from our study (450 °C, Figure 9) agrees exceptionally well with these results. The repeatability of our measurements over a range of PM samples and furnace atmosphere water concentrations indicate that monitoring CO_2 (ν_{max} 2359 and 2339 cm^{-1}, Figure 5) along with the product(s) leading to a strong hydrocarbon absorption band (ν_{max} 2968, 2933, and 2864 cm^{-1}, Figure 5) by IR absorption spectroscopy could form the basis of a sensor in a delubrication process control system. Monitoring the minor products (CH_4, C_2H_4, CO, and NH_3) seems less useful, especially since CH_4 and C_2H_4 emission maxima are well below T_c (Figure 10).

Hu and Hwang studied the dimensional changes of injection-molded iron compacts during thermal processing in an H_2 atmosphere.[18] A range of thermoplastic binders was used, but none containing any nitrogen functionality. Changes in compact elemental nitrogen, oxygen, and carbon composition were measured after heating to 370 °C. While only approximately 27 and 15 wt pct of the oxygen and carbon, respectively, were removed from the compact, 99 wt pct of the nitrogen was lost. These results suggest that the low levels of NH_3 observed here could be due to the reduction of iron-nitrogen species (*i.e.,* from the iron powder) rather than products of delubrication.

B. *High-Temperature (450 °C to 850 °C) Product Emission Modes*

While the emission profile of the long-chain hydrocarbon-containing products appears to be primarily a single-mode event peaking at 450 °C, CO and CO_2 emissions appear to follow multimode phases (Figure 11). Carbon dioxide emissions in the 200 °C to 850 °C range were found to be trimodal (maxima at 450 °C, 700 °C, and 850 °C) with ever decreasing peak intensities. Carbon monoxide production was observed as a bimodal phenomenon with a weak first peak intensity at 450 °C (11 Vol ppm in Figure 11), but a very strong second emission peak at 825 °C (424 Vol ppm in Figure 11). Emissions of CH_4, C_2H_4, and NH_3 appeared to be negligible at higher temperatures.

Danninger and Gierl employed mass spectrometry in combination with thermogravimetry to follow the evolution of gaseous products and weight loss, respectively, upon heat-treating iron (1 wt pct C) PM compacts under a helium atmosphere.[19] They observed three temperature ranges associated with weight loss and concomitant emission of gaseous compounds. Water (m/z 18, M^+) was released with emission maxima at 150 °C and 450 °C, presumably *via* desorption and the decomposition of metal hydroxides.[19] Carbon dioxide (m/z 44, M^+) was detected with a pronounced emission maximum in the 350 °C to 400 °C range. The temperature range of the second window, 680 °C to 750 °C, coincided with a pronounced mass loss and the emission of a gas with a molecular mass of 28, attributed to CO, since molecular nitrogen (N_2)—the other possible product with a molecular mass of 28—seemed less likely to form under these conditions. More mass loss was observed between 950 °C and 1100 °C and was associated with further emission of CO. These observations largely agree with ours.

The observed CO emissions in the temperature window between delubrication and sintering could have two distinct sources. The first source could be lubricant pyrolysis, with subsequent trapping of CO and CO_2 in the part's pores. This would not be unexpected because "green" part density is known[5] to affect the diffusion kinetics of gaseous species from inside the part to the surface; the higher the density, the higher the temperature of maximum weight loss. Assuming trapped CO_2 and CO are released in the 700 °C to 850 °C window, the higher relative CO concentrations compared to the first emission mode at 450 °C can be explained using a thermodynamic argument. The Gibbs free energy of the graphite-mediated reduction of CO_2 (Eq. [1]) can be calculated conveniently as a function of temperature using the Ellingham expression given in Reaction [2]:[20]

$$C\ (s) + CO_2\ (g) \rightarrow 2CO\ (g) \qquad [1]$$

$$\Delta G^\circ = 170{,}700 - 174.5T \qquad [2]$$

where ΔG° is the change in Gibbs free energy (J) at temperature T (K) for Reaction [1]. According to Reaction [2], the process shown in Reaction [1] only becomes thermodynamically feasible above 700 °C, and reaches -25.3 KJ-mol^{-1} at 850 °C. While it is acknowledged that this approach makes a number of assumptions—including equilibrium conditions—that may not fully be satisfied in the studied system, it does provide a rationale for the observed CO/CO_2 ratio emitted in the 700 °C to 850 °C window, should those gases

originate from lubricant pyrolysis. Note that there is no significant increase of large-molecule emissions in the 700 °C to 850 °C range (Figure 11), suggesting that these species remain trapped in the part. This observation is supported by the fact that 100 pct of the theoretical weight loss, calculated from the mass of lubricant used in compaction, is never obtained during delubrication.

Another explanation for the formation and release of CO above 700 °C is largely independent of the lubricant and involves surface chemistry[19] responsible for oxidizing graphite to CO. Carbon is a common alloying element and is routinely admixed with iron powders prior to compaction, as was the case in our samples (Table I). Carbon diffuses rapidly into the iron matrix upon heat treatment and it is thought[19] that dissolution may in certain instances occur immediately after the ferrite-austenite (α-γ) transition, which is at approximately 730 °C for iron containing 0.8 pct carbon.[19] Though the nature of the, potentially catalytic, surface oxidants in the putative formation of CO from graphite currently is not known, this mechanism cannot be ruled out.

Irrespective of the mechanism for CO formation in the second observed CO emission mode, it is likely that at least one mole of graphite is consumed for every two moles of released CO, per Reaction [1]; two moles of graphite will be consumed for every two moles of CO produced if iron oxides effect the oxidation. This will result in removal of the carbon dopant. For pre-sintered materials that are subsequently repressed, resized, or machined, the extent of carbon dissolution may be of considerable importance with respect to the parts' mechanical properties.[19] Thus, the second CO emission mode provides another important process parameter that could be monitored in conjunction with the delubrication indicators discussed previously.

The formation and emission of iron pentacarbonyl [$Fe(CO)_5$] in the processing atmosphere could conceivably be expected, especially during the second emission mode of CO. Iron pentacarbonyl is a relatively low boiling (bp 103 °C) compound and would be fully gaseous under the employed conditions. It is also highly toxic and its potential presence in the furnace exhaust stream is a cause for concern. However, we did not detect the presence of $Fe(CO)_5$ (ν_{max} 2000 cm^{-1}, CO), even in trace amounts, in the processing atmosphere.

C. *Effect of Atmosphere*

Renowden and Pourtalet reported[8] that water vapor in the heat-treatment atmosphere had a negative effect on lubricant removal, whereas Nayar[21] recommended a high dewpoint in the first zone of the furnace. Hwang and Lin found that the debinding rate of iron-phosphorous powder compacted with a range of lubricants was unaffected by the water vapor content of the atmosphere, although a high dewpoint prevented the formation of carbon soot on the part.[22] Our results indicate that, for the range of employed conditions, the water content of the processing atmosphere has no appreciable effect on the delubrication chemistry. Both hydrated and anhydrous processing atmospheres lead to bimodal CO emissions. However, the magnitude of the second maximum doubles in the presence of water and appears to be shifted to slightly higher temperatures. This may be due to a cooling effect of the H_2O gas, since N_2 is a poor heat-transfer medium compared to H_2O.

Thermal processing of the iron-EBS compacts in a pure N_2 atmosphere (*i.e.,* no H_2) afforded intriguing results when compared to experiments using the reducing H_2-N_2 mixture. While the product distribution and T_c seemed relatively unaffected, the second CO emission mode changed substantially. In the absence of H_2, CO emissions peaked at 750 °C (compared to 825 °C in the presence of H_2) and reached levels of 3898 Vol ppm, one order of magnitude higher than those typically observed in the presence of H_2. These results indicate that dynamic adjustment of the processing atmosphere H_2 content combined with a process control system providing feedback on the emitted CO levels may allow adjustment of the carbon removal rate from the PM compact prior to sintering.

D. *Identity of Large-Molecule Products*

One of the fundamental unsolved elements of stearate-based lubricant pyrolysis in the heat treatment of PM compacts is the chemical identity of the large-molecule products formed upon delubrication. In 1977, Ward reported results on the decomposition characteristics of these common lubricants, both as free compounds as and within iron PM compacts, in a reducing atmosphere consisting of 10 pct H_2 in N_2.[23] He found that an initial decomposition reaction—generally completed below 500 °C—yielded product(s) that contained the majority of the lubricant mass and readily condensed as a white powder in the furnace exhaust stream. Elemental analysis on the decomposition product from zinc stearate suggested that it consisted of an alkane (C_nH_{2n+2}). Although Ward suspected hexadecane ($n = 16$) or hepatdecane ($n = 17$) as likely candidates based on the structure of the hydrocarbon chain in stearates, the white solid's melting point was approximately 40 °C too high. Meyer *et al.* also reported a melting point in the 50 °C to 80 °C range for the condensable product(s) collected upon thermal processing of iron compacts lubricated with a range of stearates.[17] Bondarenko *et al.* discussed the thermolysis of zinc stearate and concluded that the principal reaction products consisted of a series of C5-C6 alkanes and alkenes and to C6-C10 ketones and ketenes.[3]

Our measurements indicate that three major large-molecule products are formed in the pyrolysis of iron-EBS compacts, along with five minor products (Table II). Further discussion is provided in Section E of possible reaction mechanisms.

E. *Reaction Mechanisms*

The reaction mechanism describing EBS pyrolysis has received little or no attention. Ward suggested[23] that stearamide thermolyzes to afford the corresponding amide radical [CH_3 $(CH_2)_{16}$ $\dot{C}ONH$], which subsequently "breaks down in the later stages of the removal of the hydrocarbon chain. This produces nascent nitrogen which could be adsorbed by or react with the iron-powder surface and inhibit sintering by surface diffusion."[24] However, Ward does not present experimental data nor literature precedents to justify this tenuous conclusion. The mechanistic discussions presented subsequently are supported by extensive experimental data, product analysis, and relevant accounts from the literature.

The first step in the pyrolysis of EBS, a long-chain secondary di-amide (Figure 1), appears to involve competition

between hydrolysis[25] (Reaction [3], R=$C_{17}H_{35}$) and *cis*-elimination *via* γ-H abstraction[26–30] (scheme 1).

$$RC(O)N(H)CH_2CH_2N(H)C(O)R + 2H_2O \rightarrow RCO_2H + H_2NCH_2CH_2N(H)C(O)R \quad [3]$$

Amide hydrolysis also could be mediated by surface iron oxides/hydroxides, with concomitant reduction of the oxide sites to metallic iron (R=$C_{17}H_{35}$):

$$RC(O)N(H)CH_2CH_2N(H)C(O)R + Fe_2O_3 + 3H_2 \rightarrow RCO_2H + H_2NCH_2CH_2N(H)C(O)R + 2Fe + 2H_2O \quad [4]$$

Drying an iron-EBS compact in the furnace at 150 °C for 8 hours prior to heat treatment under anhydrous conditions appeared to afford the same results as when an atmosphere presaturated with water vapor was employed without predrying the PM compact. These results suggest that hydrolysis occurs *via* a metal-mediated process.

Stearic acid ($C_{15}H_{35}CO_2H$, expected *m/z* 284.5, M^+, expected ν_{max} 3600, OH, 1775 cm^{-1}, C=O) is one of the two hydrolysis products, as shown in Reaction [4], but was not conclusively identified in the furnace exhaust, suggesting decomposition prior to emission; trace amounts may be present (Figure 8 and Table IV), but these data are inconclusive. This is not surprising since stearic acid and its salts have been used extensively as lubricants in the PM industry and are well known[4,23] to decompose at around 450 °C.

Pyrolysis of stearic acid potentially can proceed *via* the pathways shown in scheme 2. Pathway D, affording heptadecane (10) and CO_2 by decarboxylation, seems likely based on our experimental evidence (Table II, Figures 5, 7, and 8) and literature precedents.[31–35] However, decarboxylation of simple aliphatic acids, except for acetic acid, is known to be inefficient,[32] explaining the modest CO_2 yields (average 14 pct, assuming one mole of stearic acid for every one mole of EBS and 0.36 g of EBS in the pyrolyzed compacts) observed here. However, these yields may be significantly higher if the CO emissions observed in the 700 °C to 850 °C range can be attributed to lubricant decomposition, as discussed previously. Decarboxylation is likely to be the only significant reaction pathway in the pyrolysis of EBS-iron compacts that proceeds *via* a free radical mechanism.[33,35] Fragmentation of intermediate radical species may also explain the formation of the minor products containing less than 17 carbon atoms (Table II).

The decarbonylation of carboxylic acids (pathway C in scheme 2) is relatively rare[36] and typically requires an acid, such as sulfuric acid.[37] Heptadecanol (**9**) does not appear to form according to GC/MS, probably ruling out pathway C.

The dehydration of carboxylic acids to ketenes (route A in scheme 2) is known to occur upon pyrolysis and competes with decarboxylation; Blake and Hole observed methylketene from propionic acid in the 496 °C to 580 °C range.[33] However, ketene (**7**) was not observed by mass spectrometry, and the characteristic, strong IR absorption band in the 2197 to 2085 cm^{-1} range, corresponding to the out-of-phase stretch,[38] is missing from Figure 8.

Reduction of stearic acid to the corresponding alcohol, octodecanol (**8**), may be feasible under the conditions employed here. Hydrogenolysis (the reduction of fatty acids to their fatty alcohols) has been reported[39] to proceed in the presence of a range of metal-based catalysts, including copper, copper chromite, zinc and copper chromates, as well as nickel and copper chromates. However, octodecanol (*m/z* 270.5, M^+) was not observed by mass spectrometry and the iron-mediated reduction of carboxylic acids has not been reported in the literature, making route B unlikely.

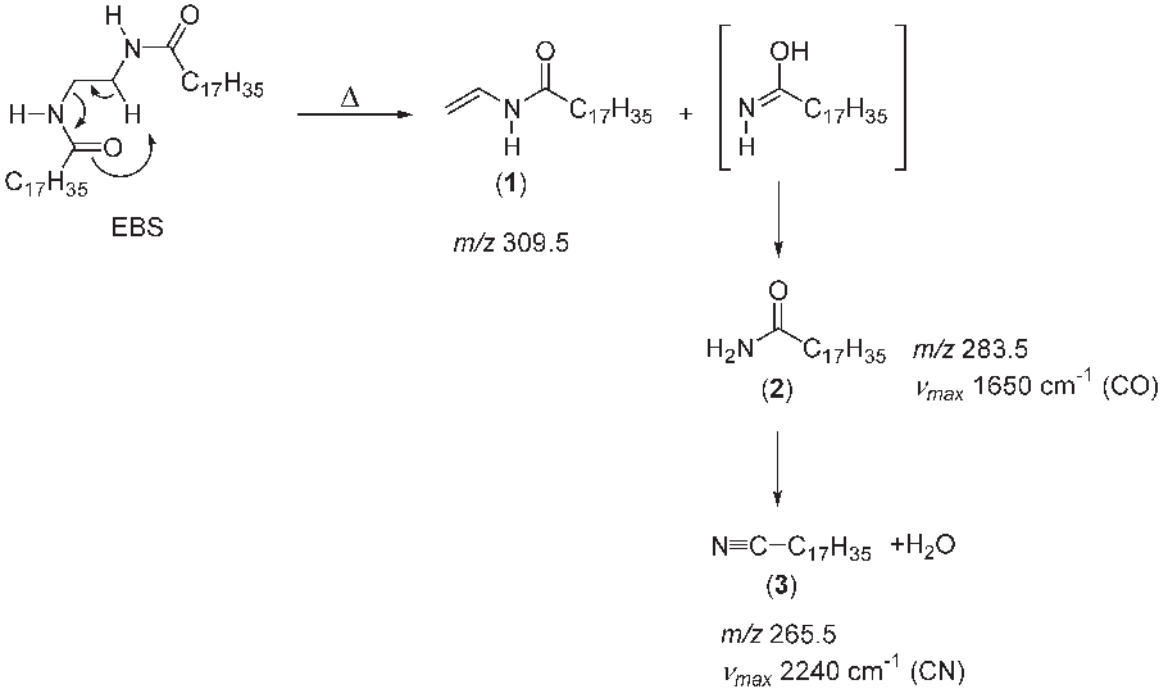

Scheme 1—Proposed *cis*-elimination of EBS.

1,2-Diamines are known[40,41] to react with carboxylic acids to yield 2-alkyl-4,5-dihydroimidazoles. 2-Heptadecyl-4,5-dihydroimidazole (**6**) can be prepared from EBS by heating for 3 days at 240 °C to 260 °C, albeit in low yield.[42] The reaction is likely to be more favorable staring with amino-amide (**4**), formed by partial hydrolysis of EBS (scheme 2). Given the evidence we have presented for the hydrolysis of EBS, Reactions [3] and [4], it is not surprising that imidazoline (**6**) is observed as a significant reaction product both by GC/MS (Table II) and by FTIR absorption spectroscopy. Interestingly, fatty 4,5-dihydroimidazoles are used widely as surface-active compounds (*e.g.,* emulsifiers and adhesive agents), but they are usually difficult to synthesize industrially.[43] Thus, the formation of imidazoline (**6**) upon the delubrication of EBS-metal compacts could represent a future recycling opportunity for the PM industry.

Table IV. IR Bands of Condensable Products of Pyrolysis Corresponding to Figure 8

Peak	Peak Location, ν_{max} (cm^{-1})	Peak Assignment[38]
A	3297	alcohol OH
B	3200	4,5-dihydroimidazole NH[43]
C	2953	alkane CH_3, asym.* vib.**
D	2917	alkane CH_2, asym. vib.
E	2848	alkane CH_2, sym.*** vib.
F	1700	carboxylic acid dimer C=O, anitsym. vib.
G	1686	amide C=O
H	1637	alkene C=C
I	1612	4,5-dihydroimidazole C=N[43]
J	1553	amide CNH, stretch-bend
K	1472	alkane CH_3, asym. bend alkane CH_2, sci.**** amide CNH, stretch-bend
L	1286	amide CNH, stretch-open carboxylic acid dimer C-OH, in-plane bend
M	972 and 898	vinyl CH wag

*asymmetric
**vibration
***symmetric
****scissor

Cis-elimination (scheme 1) of secondary amides upon pyrolysis has been shown to readily occur with *N*-alkyl-*N*-methylacetamides[27,28,29] as well as with Nylon 6,6—a polymeric amide with the [-$NH(CH_2)_6NHCO(CH_2)_4CO$-] repeat unit—and with Nylon 6,6 model systems.[44] Bailey and Bird pyrolyzed *N*-(2-acetoxyethyl)-*N*-ethylacetamide at 465 °C to afford *N*-vinyl-*N*-ethylacetamide in a 57 pct yield based on unrecovered starting material (scheme 4).[26]

Our measurements on the condensable material formed in the 400 °C to 470 °C range upon pyrolysis of iron-EBS compacts strongly suggest that *cis*-elimination as shown in Scheme 1 constitutes a primary reaction pathway. The characteristic CH out-of-plane wagging of the vinyl group (ν_{max} 972 and 898 cm^{-1}), the vinyl C=C stretch (ν_{max} 1612 cm^{-1}), and the *N*-vinyl amide carbonyl stretch (ν_{max} 1686 cm^{-1}) are all observed by IR absorption spectroscopy (Figure 6 in the gas phase and, to a lesser extent, Figure 8 and Table IV in the condensed phase). However, *N*-vinylstearamide (**1**, *m/z* 309, M^+) was not identified by GC/MS, which is not unexpected as *N*-vinylamides are prone to polymerization. This could result in material buildup in the furnace cool zone.

N-vinylstearamide (**1**) and stearamide (**2**) are expected to form in equimolar amounts upon *cis*-elimination of EBS (scheme 1). Trace amounts of amide (**2**) may have been identified by FTIR absorption spectroscopy (Figure 8 and Table IV, ν_{max} 1637 cm^{-1}, C=O), although not conclusively. Despite the absence of the characteristic, strong nitrile C≡N stretch in the mid-IR (2250 to 2230 cm^{-1}),[38] it appears that dehydration of stearamide (**2**) to octadecanenitrile (**3**) (scheme 1) occurs based on the conclusive GC/MS data in Table II. The missing IR peak likely is obscured by a water line. Primary amides are known to dehydrate to the corresponding nitrile upon pyrolysis.[30,44]

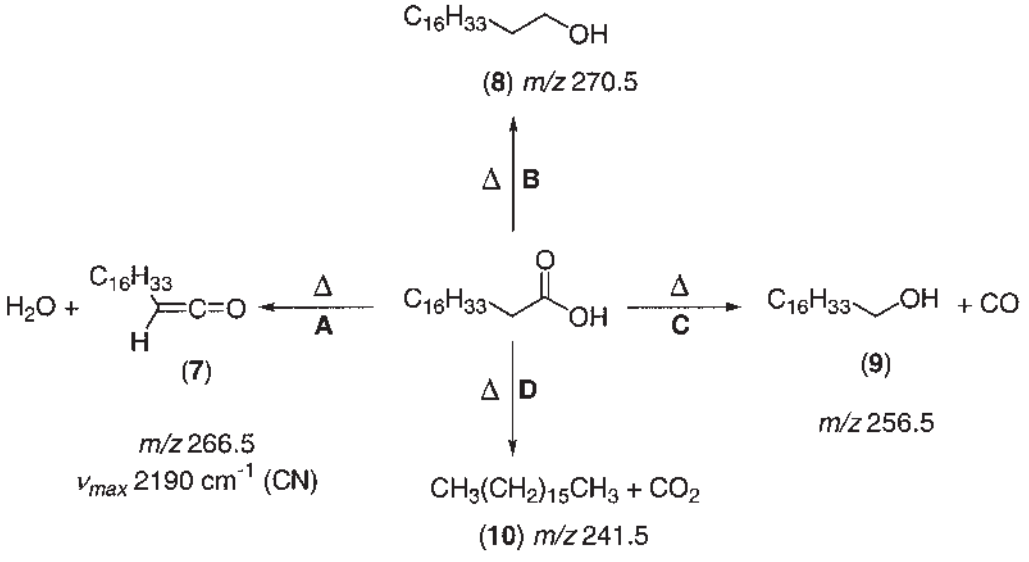

Scheme 2—Potential pyrolysis pathways for stearic acid.

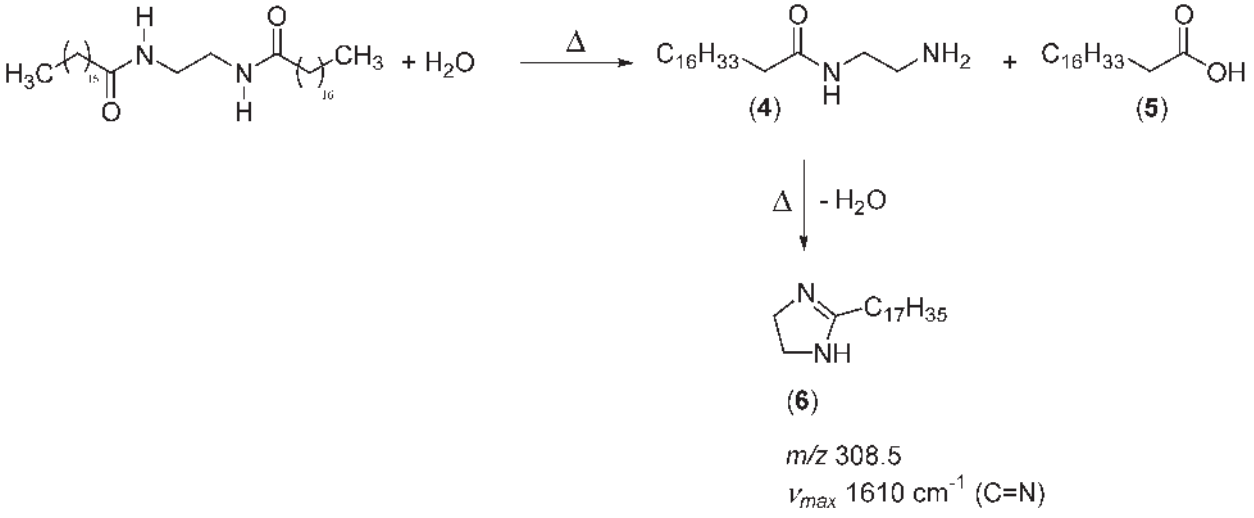

Scheme 3—Hydrolysis of EBS and imidazoline formation.

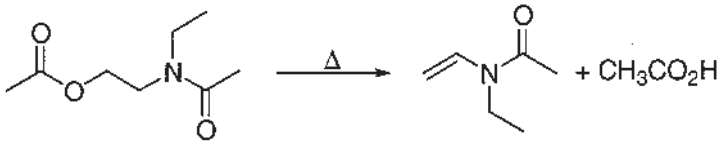

Scheme 4—Pyrolysis of an ester-amide to afford a vinyl amide.

V. CONCLUSIONS

The chemistry surrounding the pyrolysis of EBS-iron compacts is described for the first time. A wide range of analytes emitted from this process were measured by FTIR absorption spectroscopy and by GC/MS. The aliphatic CH stretch in the 3000 to 2700 cm^{-1} range and the asymmetric CO stretch in CO_2 at 2350 cm^{-1} are excellent indicators of delubrication. A bimodal CO emission phase was observed in the temperature window between delubrication and sintering, which was severely affected by the H_2 content of the furnace atmosphere. Based on our results, a process sensor monitoring the hydrocarbon CH stretch and CO_2 to control delubrication, and CO to tune the part C content, would appear to hold much potential for the PM industry.

Three major large-molecule reaction products, along with five minor compounds were identified by GC/MS. A preliminary reaction mechanism was inferred based on product analysis and known organic chemistry. It appears that hydrolysis of EBS competes with γ-H abstraction yielding an *N*-vinyl amide and stearamide, which undergoes further reaction. Hydrolysis affords stearic acid, which decarboxylates to heptadecane, and 2-heptadecyl-4,5-dihydroimidazole *via* a ring closure of the corresponding amino-amide. Our results set the foundation for the future work aimed at tuning the lubricant functionality to control its pyrolysis in terms of the characteristic temperature and the nature of the products.

Future efforts will focus on further elucidating the reaction mechanism and kinetics of EBS pyrolysis, as well as identifying the role of the metal in these processes. The surface chemistry of the iron compact also will be investigated. A spectroscopic sensor, along with a process control feedback model, currently is under development to allow the efficient management of the presintering conditions in industrial furnaces.

ACKNOWLEDGMENTS

The authors are grateful to the PMRC members for their support and thank Mr. Fred Semel (Hogaenaes Corp.) for providing compacted samples during the course of this study. The authors also thank Dr. Nathan F. Dalleska, Division of Environmental Science and Engineering, California Institute of Technology (Pasadena, CA), for helpful discussions regarding the interpretation of GC/MS data.

REFERENCES

1. J. Auborn: *Mechanisms of Lubrication in Powder Metallurgy,* Metal Powder Industries Federation, Princeton, NJ, 1993, vol. 2, pp. 17-25.
2. R.M. German: in *Thermal Extraction of Binders and Lubricants in Sintering,* T. Cadle and K.S. Narasimhan, eds., Metal Powder Industries Federation, Princeton, NJ, 1996, vol. 3, pp. 10-13-10-16.
3. B.I. Bondarenko, I.V. Voloshin, Y.A. Voloshina, V.D. Artemev, L.E. Rubinchik, and S.G. Ruzhanskii: *Powder Metall. Met. Ceram.,* 1993, vol. 32, pp. 461-64.
4. J. McGraw, M.J. Koczak, and A. Kao: *Int. J. Powder Metall.,* 1978, vol. 14, p. 277.
5. D. Saha and D. Apelian: *Int. J. Powder Metall.,* 2002, vol. 38, pp. 71-79.
6. D. Saha, M.M. Baum, and D. Apelian: *Int. Conf. on Powder Metallurgy and Particulate Materials,* Proc. Int. Conf. on Powder Metallurgy and Particulate Materials, New Orleans, LA, May 13–17, 2001, MPIF, Princeton, NJ, 2001, pp. 82-94.
7. J.U. White: *J. Opt. Soc. Am.,* 1942, vol. 32, pp. 285-88.
8. M. Renowden and P. Pourtalet: in *Experimental Studies on Lubricant Removal,* E.R. Andreotti and P.J. McGeehan, eds., Metal Powder Industries Federation, Princeton, NJ, 1990, vol. 1, pp. 261-78.

9. M.M. Baum, E.S. Kiyomiya, S. Kumar, A.M. Lappas, and H.C. Lord, III: *Environ. Sci. Technol.,* 2000, vol. 34, pp. 2851-58.
10. M.M. Baum, E.S. Kiyomiya, S. Kumar, A.M. Lappas, V.A. Kapinus, and H.C. Lord, III: *Environ. Sci. Technol.,* 2001, vol. 35, pp. 3735-41.
11. M.M. Baum, S. Kumar, A.M. Lappas, and P.D. Wagner: *Rev. Sci. Instrum.,* 2003, vol. 74, pp. 3104-10.
12. J.N. Pitts, Jr., H.W. Biermann, A.M. Winer, and E.C. Tuazon: *Atmos. Environ.,* 1984, vol. 18, pp. 847-54.
13. J. Mellqvist and A. Rosén: *J. Quant. Spectrosc. Radiat. Transfer,* 1996, vol. 56, pp. 209-24.
14. L.C.K. Liau, B. Peters, D.S. Krueger, A. Gordon, D.S. Viswanath, and S.J. Lombardo: *J. Am. Ceram. Soc.,* 2000, vol. 83, pp. 2645-53.
15. R.V. Shende and S.J. Lombardo: *J. Am. Ceram. Soc.,* 2002, vol. 85, pp. 780-86.
16. G. White and H. Nayar: in *Monitoring of the Delubrication Process under Production Conditions,* T. Cadle and K.S. Narasimhan, eds., Metal Powder Industries Federation, Princeton, NJ, 1996, vol. 3, pp. 10-27-10-40.
17. R. Meyer, J. Pillot, and H. Pastor: *Powder Metall.,* 1969, vol. 12, pp. 298-304.
18. S.C. Hu and K.S. Hwang: *Powder Metall.,* 2000, vol. 43, pp. 239-44.
19. H. Danninger and C. Gierl: *Mater. Chem. Phys.,* 2001, vol. 67, pp. 49-55.
20. D.R. Gaskell: *Introduction to Thermodynamics of Materials,* 3rd ed., Taylor & Francis, New York, NY, 2003.
21. H.S. Nayar: *Production Sintering Atmospheres,* 9th ed., ASM, Metals Park, OH, 1984, vol. 7, p. 340.
22. K.S. Hwang and K.H. Lin: *Int. J. Powder Metall.,* 1992, vol. 28, pp. 353-60.
23. M. Ward: *Int. J. Powder Metall.,* 1977, vol. 13, pp. 197-214.
24. M. Ward: *Powder Metall.,* 1979, vol. 22, pp. 193-200.
25. N.O.V. Sonntag: *Nitrogen Derivatives,* 2nd ed., K.S. Markley, ed., Fats and Oils, Interscience, New York, NY, 1964, vol. 3, pp. 1551-1715.
26. W.J. Bailey and C.N. Bird: *J. Org. Chem.,* 1958, vol. 23, pp. 996-1001.
27. H.E. Baumgarten, F.A. Bower, R.A. Setterquist, and R.E. Allen: *J Am. Chem. Soc.,* 1958, vol. 80, pp. 4588-93.
28. A. Maccoll and S.S. Nagra: *J. Chem. Soc.-Faraday Trans. I,* 1973, vol. 69, pp. 1108-16.
29. A. Maccoll and S.S. Nagra: *J. Chem. Soc.-Faraday Trans. I,* 1975, vol. 71, pp. 2450-58.
30. R. Taylor: in *Pyrolysis of Acids and Their Derivatives,* S. Patai, ed., The Chemistry of Functional Groups, John Wiley & Sons, New York, NY, 1979, vol. 2, pp. 859-914.
31. N.O.V. Sonntag: in *Dehydration, Pyrolysis, and Polymerization,* 2nd ed., K.S. Markley, ed., Fats and Oils, Interscience, New York, NY, 1961, vol. 2, pp. 985-1072.
32. J. March: *J. Chem. Ed.,* 1963, vol. 40, pp. 212-13.
33. P.G. Blake and K.J. Hole: *J. Chem. Soc. B-Phys. Org.,* 1966, vol., pp. 577-79.
34. L.W. Clark: in *The Decarboxlation Reaction,* S. Patai, ed., The Chemistry of Functional Groups, John Wiley & Sons, New York, NY, 1969, pp. 589-622.
35. K.R. Doolan, J.C. Mackie, and C.R. Reid: *Int. J. Chem. Kinet.,* 1986, vol. 18, pp. 575-96.
36. J. March: *Advanced Organic Chemistry,* 3rd ed., John Wiley & Sons, New York, NY, 1985, pp. 1346.
37. M. Zielinski: in *Synthesis and Uses of Isotopically Labeled Carboxylic Acids,* S. Patai, ed., The Chemistry of Functional Groups, John Wiley & Sons, New York, NY, 1969, pp. 453-503.
38. D. Lin-Vien, N.B. Colthup, W.G. Flateley, and J.G. Grasselli: *The Handbook of Infrared and Raman Characeristic Frequencies of Organic Molecules,* Academic Press, San Diego, CA, 1991.
39. K.S. Markley: in *Hydrogenation,* 2nd ed., K.S. Markley, ed., Fats and Oils, Interscience, New York, NY, 1961, vol. 2, pp. 1187-1305.
40. J.L. Riebsomer: *J. Am. Chem. Soc.,* 1948, vol. 70, pp. 1629-32.
41. R.J. Ferm and J.L. Riebsomer: *Chem. Rev.,* 1954, vol. 54, pp. 593-613.
42. R.N. Butler, C.B. Oregan, and P. Moynihan: *J. Chem. Soc.-Perkin Trans. 1,* 1976, pp. 386-89.
43. R.N. Butler, J.D. Thornton, and C.B. Oregan: *J. Chem. Soc.-Perkin Trans. 1,* 1983, pp. 2197-200.
44. M.A. Schaffer, E.K. Marchildon, K.B. McAuley, and M.F. Cunningham: *J. Macromol. Sci.-Rev. Macromol. Chem. Phys.,* 2000, vol. C40, pp. 233-72.